STEND: Stimulated emission non-linear-depletion super-resolution microscopy

GYANENDRA SINGH,[1] YOSSI MOSBACHER,[1,2] RANIT ROY,[1] DROR HERSHKOVITZ,[1] GUY PAISS,[1] AND O. CHESHNOVSKY [1*]

[1] *School of Chemistry, The Raymond and Beverly Sackler Faculty of Exact Sciences, Tel Aviv University, Tel Aviv 69978, Israel, the Tel Aviv University center for Nanoscience and Nanotechnology and the Tel Aviv University center for Light Matter Interactions.*
[2] *Department of Particle Physics and Astrophysics, Weizmann Institute of Science, Rehovot, Israel*
**Corresponding author: orich@tauex.tau.ac.il*

Abstract: We introduce a novel method for achieving super-resolution (SR) in fluorescence microscopy, based on the nonlinear reduction of fluorescence by stimulated emission depletion (STED). This nonlinearity is used to couple the high spatial-frequency components of the fluorescence image to harmonics of fluorescence response to STED intensity modulation. Both the excitation and the modulated STED laser beams are co-focused to diffraction limited spots and scanned over the sample. The harmonic content is extracted using lock-in demodulation techniques. The demodulated point spread function of harmonic *n*, improves in resolution like $\sqrt{n}$. Using fluorescent nano-diamonds, we demonstrate SR with lateral and axial resolutions of 113 ± 20 nm and 330 ± 20 nm respectively, for $n = 4$. This methodology can be easily adapted to any scanning confocal microscope and pulsed beams.

1. Introduction

The advent of optical super resolution (SR) microscopy during the last two decades has dramatically enhanced the merits of fluorescence microscopy in biological research [1,2]. Cellular structure and organization of fixed or live cells can be deciphered down to tens of nanometres. Optical microscopy has succeeded in surpassing the Abbé resolution limit (~0.5λ) [3] either by near-field techniques [4], or by far-field super-resolution (SR) techniques such as stimulated emission depletion (STED) [5,6], photo-activated localization microscopy (PALM), stochastic optical reconstruction microscopy (STORM) [7,8], saturated absorption (SAX) [9], structured illumination [10], SR optical fluctuation imaging (SOFI) [11], and quantum emitters microscopy [12]. The advent of algorithmic approaches and sophisticated image analysis has further supported the enhancement of resolution [13]. The achievement of SR does not come without penalties. Each SR method suffers from a unique set of shortcomings as compared to confocal microscopy in various metrics such as: axial (Z) resolution, lateral (X, Y) resolution, sample thickness, live-cell cytotoxicity, image fidelity, multicolor, temporal resolution, availability (cost), and versatility [1].

Multiple approaches for achieving SR by exploiting nonlinearities in fluorescence or light scattering were introduced during the last two decades. Gustafsson has advanced the idea of using the nonlinearity of fluorescence induced by saturation to surpass the factor 2 improvement intrinsic to SIM [14]. Soon after, Fujita and co-workers have proposed to use saturable

excitation (SAX) to achieve SR [9], and demonstrated its efficacy in imaging biological systems [15]. Taki and co-workers have extended the idea of SAX to the time domain, by using pump and depletion (STED) co-focused beams [16,17]. They have modulated both the excitation beam and the STED beam. By measuring the second order nonlinearity in the fluorescence in relation to the excitation beam, they showed distinct improvement in resolving 500nm fluorescent beads, like in SAX. However, they did not report resolution improvement beyond the diffraction limit. While attributing the improvement in resolution to repetitive simulated transition (REST), the nonlinear dependence on the excitation intensity was demonstrated, as in SAX. Dake and Hayashi has used the same experimental methodology and showed resolution improvements that depends on the second order of the STED beam [18]. As we show, this nonlinearity is intrinsic to the STED process. In their works higher-order dependence of either excitation or STED beams or both were not reported, and therefore, in our view, their mechanism for resolution improvement has not been proved.

In addition to fluorescence-based approaches, Chu and co-workers utilized the nonlinear nature of plasmonic scattering for achieving SR [19]. The equivalent label-free approach has been developed by Cheshnovsky and co-workers using a pump and probe scheme [20,21]. Nonlinear photo-modulated reflectivity (NPMR) for far-field, label-free, SR microscopy is based on measuring (with a probe beam) the nonlinear changes in the reflectance of materials, induced by earlier ultra-short pump pulse excitation.

The dynamic response of fluorescence in STED nanoscopy has also been utilized to enhance the resolution and remove anti-Stokes background. Such methods include temporal modulation of the excitation beam [22], the more sophisticated FPGA-STED approach where a pixel-based subtraction method is used for better demodulation in removing anti-Stokes emission background [23], or the FLIM-STED approach, where the lifetime information is used for demodulation [24].

Here, we propose to modulate a Bessel STED beam and to exploit the high intrinsic nonlinearity of the fluorescence yield, induced by STED, to achieve SR. Technically this work is similar to REST. We use co-focused excitation and STED beams. The modulated STED beam depletes the emission only partially (20-50%). By doing so, we reduce dramatically the potential of photo-induced damages caused by the strong depletion beam in STED microscopy or by the strong excitation required by SAX. An advantage of not using a vortex STED beam, which deteriorates fast in turbid biological samples, is the increased depth of the interrogation without the need of adaptive wave front corrections [25].

2. Stimulated emission non-linear-depletion (STEND), concept and modeling

In our method, we excite the sample with a focused pump beam, while a pure sine wave STED beam modulates its fluorescence. The point spread function (PSF) of the modulated fluorescence is a product of the PSFs of the pump and the modulating STED beam. The key to SR are the high order components of the Stimulated Emission Nonlinear Depletion (STEND). . The PSF of the *n-th* nonlinear order, $PSF_{STEND}(n)$ can be expressed as $PSF_{STEND}(n) = PSF_{STED}^{n} \times PSF_{p}$., where PSF_p and PSF_{STED} are the PSF of the pump and the STED beams respectively. As the resolution of STEND scales with the power n of PSF_{STED}, the achievable resolution will highly benefit from narrowing its width. Thus, we have chosen to use a Bessel beam for the STED, while maintaining the shorter wavelength excitation-beam Gaussian. Such a strategy results in improved lateral SR while maintaining the vertical resolution practically intact, as in conventional confocal microscopy.

The simulated PSFs of STEND are depicted in Fig.1. We simulate the relevant laser beams of our experiment: A Gaussian excitation beam at 532 nm and a Bessel beam at 730 nm both focused through a 1.35 NA objective. In practice, extracting the *n*-th order of the modulated fluorescence is accomplished by measuring the *n*-th harmonic of the fluorescence signal. The simulated FWHM of the PSF are 250nm, 250nm, 181nm, 118nm and 89 nm for the Gaussian beam, Bessel beam (central lobe), and the first, fourth and eight harmonics respectively. Note in Fig. 1 that the wings of the Bessel beam do not overlap the Gaussian excitation beam, and therefore do not contribute to the modulated signal.

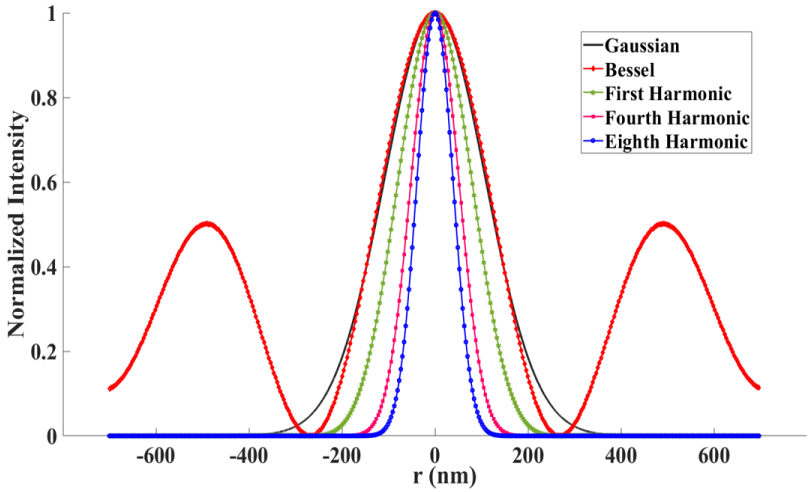

Fig. 1. Model PSFs in the STEND microscopy. (Gray) of the excitation Gaussian beam; (Red, Diamond) the STED Bessel beam; The Green (Star), Pink (Square), and Blue (Circle) lines represent the PSFs of the modulated fluorescence in the first, fourth and eighth order respectively. Note that the wings of the Bessel beam do not overlap the excitation and do not contribute to the modulated fluorescence.

In what follows, we present briefly the results of a theoretical model showing how STEND achieves SR (see the section titled "Theoretical model of STEND" of the supplementary material). We refer to the photo-physics of nitrogen vacancy (NV) diamonds [26].While the details of the photophysics dynamics vary with the nature of the color-center and the wavelengths of the excitation and STED beams, we show that the competition between the stimulated depletion the emission and other quenching processes leads to highly nonlinear dependence of the fluorescence yield on the STED beam intensity. We analyse a CW-laser scheme, yet extensions to include pulsed excitation and STED beams are simple.

Although fluorescent nano diamonds (FNDs) were used in the current study, any other chromophores, suitable for STED microscopy and characterized by similar dynamics, are suitable for STEND. The photo-physics of NV diamonds in STED nanoscopy have been studied extensively [27,28,29]. We extend our treatment to include the accumulation of population in the long lived ^{1}E state. The most relevant energy levels for our SR methodology with NV diamonds are the $^3A_2$ ground state, the optically excited ^{3}E state, and the ^{1}E singlet level, which is radiatively fast populated by $^1A_1$ level, populated by intersystem crossing from the ^{3}E excited states. (See insert in Figure 2) [30]. To make the discussion general, we will refer to $^3A_2$, ^{3}E, and ^{1}E states as the ground state G, excited state E and intermediate state IS respectively.

The rate equation for the population of the excited state can be described as follows:

$$\frac{dG}{dt} = -k_{ex}[G] + k_{rad}[E] + k_{STED}[E] + k_{ISC(IS\to G)}[IS], \quad (1)$$

$$\frac{dE}{dt} = +k_{ex}[G] - k_{em}[E] - k_{STED}[E], \quad (2)$$

$$\frac{d[IS]}{dt} = -k_{ISC(IS\to G)}[IS] + k_{ISC(E\to 1A1)}[E], \quad (3)$$

where [G] [E] and [IS] represent the normalized population of the ground, excited and intermediate state, respectively, and [G] + [E] + [IS] = 1. k_{em} is the emission lifetime and equals the sum k_{rad} and $k_{ISC(E\to 1A1)}$, representing the pure emission rate and the non-radiative intersystem crossing rate of the excited state, respectively. $k_{ISC(IS\to G)}$ represents the non-radiative intersystem crossing rate of the intermediate state to the ground state. k_{STED}, is parametrized as $\sigma_{STED} I_{STED}$, where σ_{STED} is the cross section for stimulated depletion from the excited state E. I_{STED} represents the local intensity of the STED beam. The excitation rate k_{ex} is parametrized as the product of the absorption cross section σ_{ex} and the local excitation beam intensity, I_{ex}.

In steady state for IS, and since the radiative depopulation of $^1A_1$ is fast compared to other rates, we derive the relation between [E] and [IS] to be:

$$[IS] = \frac{k_{ISC(E\to 1A1)}}{k_{ISC(IS\to G)}}[E] \equiv \gamma[E], \quad (4)$$

where γ represents the ratio of ISC rates to and from the IS, respectively. Assuming steady state for Eq. 2 we show that the emission depletion, $\eta_{CW-STED}$, induced by the STED beam in steady state is given as:

$$\eta_{CW-STED} = \frac{k_{ex}(1+\gamma) + k_{em}}{k_{ex}(1+\gamma) + \sigma_{STED} I_{STED} + k_{em}}. \quad (8)$$

Our expression includes the effect of the steady state population of the long lived IS (^1E), which causes reduced depletion efficiency by the STED beam.

We define $\sigma_{STED}/[k_{ex}(1+\gamma) + k_{em}] = \beta$ and expand Eq. 8 as a Taylor series of the parameter βI_{STED}, highlighting the nonlinear nature of the STED depletion. For $\beta I_{STED} < 1, \eta_{CW-STED}$, (Eq. 8) can be expended as:

$$\eta_{CW-STED} = (1 - \beta I_{STED} + \beta^2 I_{STED}^2 - \beta^3 I_{STED}^3 + \beta^4 I_{STED}^4 \ldots), \quad (9)$$

In order to achieve SR in the fluorescence, it is necessary to isolate the high order terms of the depletion efficiency. Isolation of the nth order term will result in an improved resolution by the n^{th} power of the STED beam PSF. We have chosen to experimentally isolate these high-order components by sine intensity-modulation ($at\ \omega_m$) of the STED beam. The modulated STED beam is focused on the sample along with the excitation beam. The time dependent fluorescence signal is collected and demodulated in real time. The nonlinear components of the fluorescence signal due to modulation (at ω_m) are demodulated at the corresponding harmonic frequencies ($\omega_m, 2\omega_m, 3\omega_m, 4\omega_m$ ...) using a lock-in amplifier.

The relations between the nonlinearity order and the harmonic components of the modulated fluorescence are presented here. We express the time dependence of the STED modulated beam as:

$$I_{STED}(t) = I_0 \frac{(1+cos\omega_m t)}{2}. \tag{10}$$

Considering the lifetime values of the relevant levels [30], we assume that steady-state formation is much faster than period of modulation (800 µs). This allows us to insert the expression of Eq. 10 to Eq. 9, resulting in time dependent $\eta_{CW-STED}(t)$:

$$\begin{aligned}&\eta_{CW-STED}= \\ &=[1-\left(\frac{1}{2}\beta I_0-\frac{3}{8}\beta^2 I_0^2+\frac{5}{16}\beta^3 I_0^3-\frac{35}{128}\beta^4 I_0^4\right)-\left(\frac{1}{2}\beta I_0-\frac{1}{2}\beta^2 I_0^2+\frac{15}{32}\beta^3 I_0^3-\frac{7}{16}\beta^4 I_0^4\right)cos\omega_m t \\ &+\left(\frac{1}{8}\beta^2 I_0^2-\frac{3}{16}\beta^3 I_0^3+\frac{7}{32}\beta^4 I_0^4\right)cos2\omega_m t-\left(\frac{1}{32}\beta^3 I_0^3-\frac{1}{16}\beta^4 I_0^4\right)cos3\omega_m t+\left(\frac{1}{128}\beta^4 I_0^4\right)cos4\omega_m t\ldots].\end{aligned} \tag{13}$$

We emphasize two conclusions from the above expansion:

A. For $\beta I_0 < 1$, namely mild STED, the intensity coefficients decrease with the n^{th} order.
B. The dominant term in each order *n*, is proportional to I_0^n . Therefore, the PSF of the n^{th} harmonics of $\eta_{CW-STED}$, $PSF_{STEND}(n)$, approximately equals:

$$PSF_{STEND}(n) = PSF_{STED}^n \times PSF_p. \tag{14}$$

In theory, as in SAX and in SOFI, resolution improvement is unlimited. However, the power content of high harmonics decreases with *n*, and the highest available order is limited and governed by the SNR and the harmonic purity of the modulated STED beam.

3. Experimental method

The experimental setup is illustrated in Fig.2. Typically, we excite the sample using 1.1 mW of a 532 nm CW laser beam (Laser Glow, LSR-0532-PFM-00100-03, > 100 mW), while STED is induced using an 11.9 mW, 730 nm CW laser beam (Oxxius Laser, LBX 730, 40 mW). Both intensities are measured at the entrance to the objective lens. The 532 nm green laser is spatially filtered with a 20 µm pinhole situated inside an 8.3X beam expander, which uses 15 mm and 125 mm focal length achromatic lenses. The Gaussian red laser beam is converted to a Bessel-Gauss beam using a 5° Axicon (Thorlabs AX125).

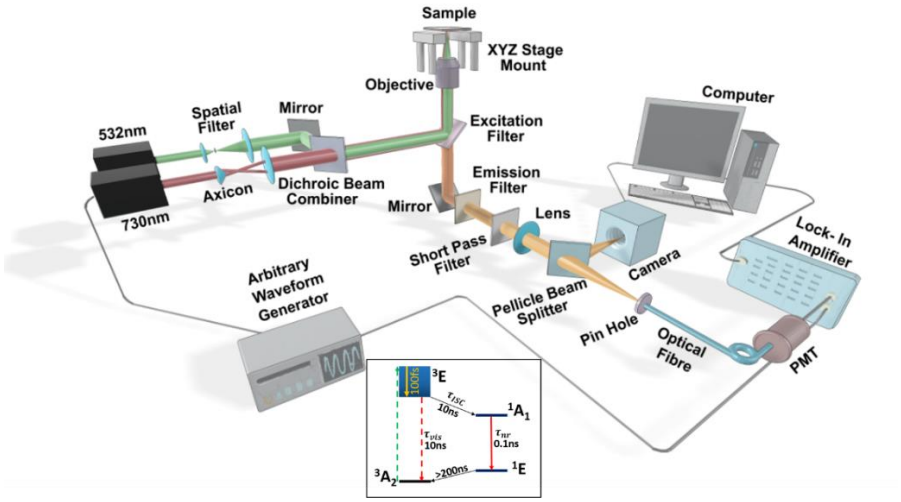

Fig. 2. Experimental set-up used for the STEND SR microscopy. The insert depicts a simplified scheme of the relevant energy levels, used in the theoretical modelling section [30].

The isolation of specific harmonics in fluorescence requires a pure sinusoidal modulation of the STED laser beam, to avoid direct modulation at high harmonics. Modulation is performed by feeding the analogue modulation input of the laser with an arbitrary waveform generator (Rigol-DG1022). A closed loop optimization algorithm (MATLAB) is implemented to produce a driving waveform that minimizes high order harmonic distortion in the STED beam intensity to less than 0.6% [31] at a modulation frequency of $\omega = 12.5$ KHz. We achieve pure sine wave modulation with high harmonics content of 0.3%, 0.18%, and 0.09% for the 2 nd, 3rd and 4th harmonics respectively. Both the excitation and STED beams are combined using the dichroic beam combiner (Chroma, T600lpxr-UF3) and are projected into the microscope objective (Olympus 60X, N.A. 1.35 Oil) through an excitation filter (Chroma, ZT405/488/543RPS-UF2) in an epi-fluorescence configuration.

The sample is mounted on an X-Y piezo stage (Micronix USA PPX-50), used to position and scan the sample, attached to a Z piezo stage (Micronix USA PPS-60) to focus the sample and provide Z scanning. The scan is performed through a 3 axes driver (Micronix USA, MMC-110) controlled by an in house Python software package, which is used also for data acquisition. Typically, raster scans of 21nm steps and 60 ms dwell time per pixel are used for imaging.

Red Fluorescent nano-diamonds, br-FND (FND Biotech) in the size range of 30-100 nm were used to prepare samples of nano-objects. They were dry spread on a marked Indium tin oxide (ITO) coated, 170 µm thick cover slip (SPI, 06462-AB). The ITO coating facilitates SEM imaging of the sample, to be compared with the optical luminescence scanned images. The epifluorescence from the sample is filtered with an emission filter (Semrock, FF01-632/148) and short pass filter (Edmund Optics, 700 nm OD4) and is focussed using a tube lens (f = 250 mm). The signal is split by pellicle to a CMOS camera (30%) (Edmund optics, E0-1312C), used for bright-field microscopy as well as for the identification of luminescent particles. 70% of the signal is collected by a multimode fibre (Thorlabs, 0.22NA, 50 µm, M14L01) and fed into a PMT (Hamamatsu, H7422P-40) for detection. The PMT signal is amplified by the pre-amplifier (Hamamatsu, C7319), then fed into a lock-in amplifier (MFLI Zurich Instrument, 500 kHz) where three of the harmonics are simultaneously demodulated. The analogue output

channels of the lock-in amplifier are fed to a data acquisition card DAQ (NI USB -6229) and are recorded using the same Python-based in-house software package. The integrated intensity of the fluorescence signal along with a selection of three of 1^{st}-5^{th} harmonics components are recorded simultaneously.

The high spatial frequency components of the high order $\eta_{CW-STED}(t)$ are attenuated in the optical transfer function (OTF), therefore the row scan data are transformed via Fourier reweighting (FRW), as practiced in several SR techniques [32, 33, 34, 35](see Supplement 1.2 for details). For the sake of clarity, we present our row scan data alongside the FRW transformed images (see supplementary materials section 1.3 for details).

4. Results and discussion

We have searched for the location of isolated FNDs applying a wide field fluorescence imaging mode. Once found, we performed modulated scans on a smaller area, typically 1×1 μm^2. To retrieve the PSF achieved with our methodology, we performed a lateral (X-Y) and axial (X-Z) scans (21nm steps) of a single nano-diamond of 50 nm (+/- 5 nm), recording simultaneously the non-modulated fluorescence component along with three demodulated fluorescence images of the 1^{st}, 3^{rd} and 4^{th} harmonics. Signals from the 5^{th} harmonics were also recorded, but their intensity strength was low and inconsistent. We have spatially demodulated the optical scan-image from the SEM image of the same individual FND, retrieving the PSF of the STEND in each harmonic (see Supplement 1.3 for details). The experimental extracted lateral PSFs are depicted in Fig. 3(a). The FWHM for the extracted lateral-PSFs are 224 ± 20 nm, 172 ± 20 nm, 125 ± 20 nm and 113 ± 20 nm, for the integrated fluorescence (with the modulated STED beam), first, third and fourth harmonics respectively. Note that these values are almost identical to the simulated values depicted in Figure 1.

Scans along the X-Z coordinates were performed over the same particle, to retrieve the axial PSFs. We have assumed in the process of the X-Z PSF extraction that the height of the FND, which cannot be deduced from the SEM image, is 50 nm, as are the other dimensions. The results are depicted in Fig. 3(b). The FWHM for the calculated PSF for the axial direction are 350 ± 20 nm, 323 ± 20 nm, 327 ± 20 nm and 329 ± 20 nm for the integrated fluorescence, first, third and fourth harmonics, respectively (see supplementary materials section 1.4 for details). The Z PSF of the fluorescence is governed by the PSF of the excitation Gaussian beam and practically does not vary for all higher harmonics images, since the overlapping Bessel STED beam is considerably larger along the Z axis.

In Fig. 3(c), we present the cross section of these PSFs along the X-axis. Note that the cross sections of the extracted PSFs along the X axis from both the XY and the XZ scans are practically identical at the same Y coordinates, demonstrating the robustness of our scans. The axial, diffraction limited profile, for the scan shown in Fig 3(b) is given in Fig. S5 (supplementary materials section).

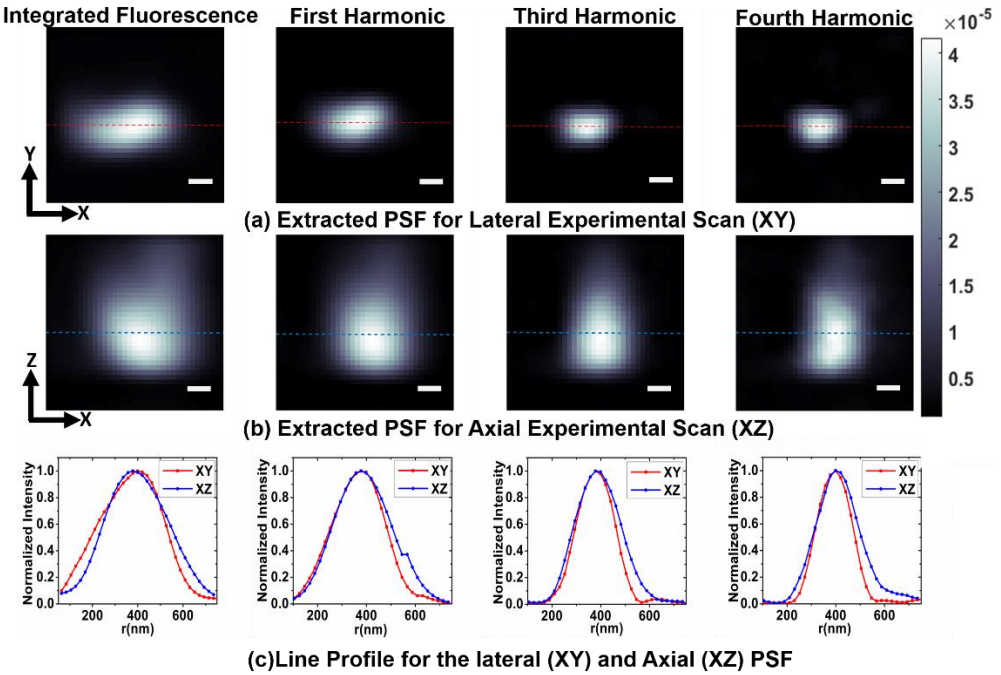

Fig. 3. Intensity-normalized PSFs of STEND at various harmonies order *n*, extracted by demodulation of the SEM image from the fluorescence STEND scanning of a 50 nm nano-diamond for the integrated fluorescence, first, third and fourth harmonics. (a) Lateral (X Y) and (b) Axial (X Z) scans. The red and blue lines mark the location of the cross-sections presented in (c). The white scale bars in (a) & (b) are 100 nm.

The real challenge, though, is to demonstrate the ability to resolve adjacent nano-objects. Figure 4 depicts a SEM image of FNDs spread on the ITO-coated substrate, marked by a mesh of lines, ablated by a laser writer. This mesh, with its unique geometric features, enabled the genuine identification of a specific group of nanoparticles. Highlighted are SEM images of two particles of average size 120 ± 20 nm and 110 ± 20 nm separated by 150 nm along with their STEND fluorescence-image generated by the 4^{th} harmonics signal. The whole set of measurements on this FNDs-pair is depicted in Fig. 5, presenting the raw data of a X-Y scan of 0.8 μm^2 with a step size of 21 nm in Fig. 5(a). Note, that while the particles are not resolved in the first harmonic, they are very clearly separated in the 4^{th} harmonics image.

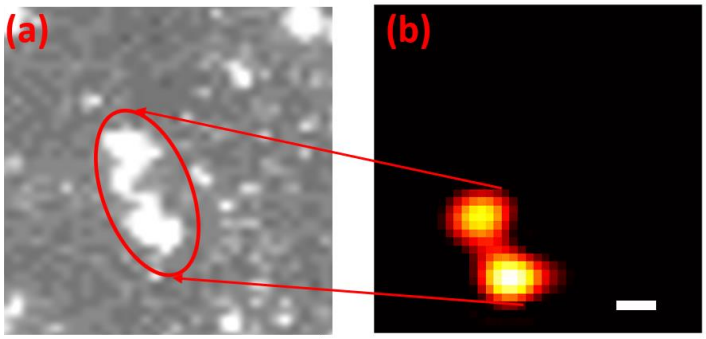

Fig. 4. (a) SEM image of two FNDs, not resolvable by confocal scanning. (b) FRW fourth harmonic STEND lateral scan. The white scale bar is 100 nm.

In the row implementation of our method, the resolution improvement scales as $\sqrt{n}$, the harmonics order. However, FRW reweighting the high frequency spatial components which have been attenuated in the scanned image, can further improve the resolution up to n [33, 34, 35] (see supplementary materials section 1.2 for details). The corresponding FRW scans are presented in Fig. 5(b).

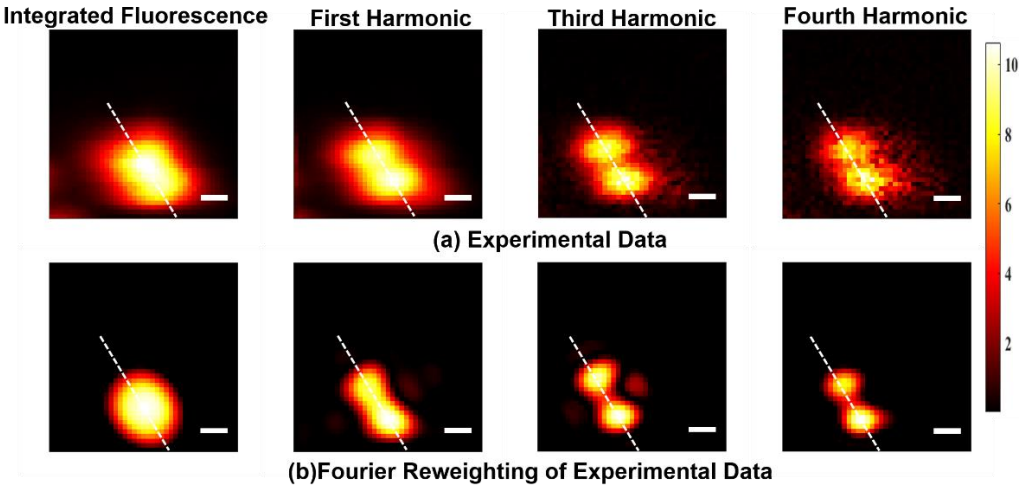

Fig. 5. (a) A 700 µ by 700µ XY scan of the nano-diamonds (b) FRW of the corresponding XY scans. The white scale bar are 100nm.

Cross-section profiles for the raw experimental data and the FRW images are shown in Fig. 6(a) and Fig. 6(b), respectively. The cross-section profiles along the white dotted lines for the scans are shown in Fig. 5(a) and Fig. 5(b). The measured de-convolved size of the nano-diamonds from the FRW is 120 ± 20 nm and 110 ± 20 nm. As expected, the FRW data shows better resolution, and the two FND situated 150 nm apart are well resolved in the 4th harmonic images. For X-Z scan for the two particles, with the same lateral resolution, see supplementary materials section 1.5.

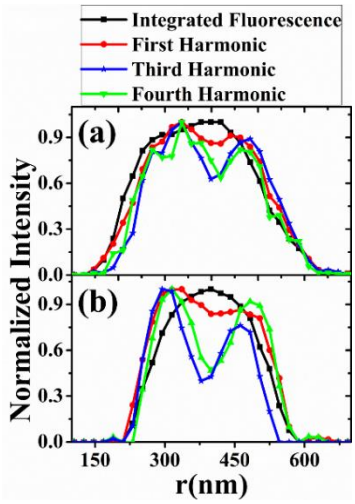

Fig. 6. Cross-section line profile for: (a) the row experimental scanned data depicted in Fig. 5(a). (b) The FRW data depicted in Fig. 5(b).

5. Conclusions

In summary, we have introduced a new SR-modality, utilizing stimulated emission depletion. Unlike the original STED microscopy that depends on a vortex beam, our Gaussian depletion beam is co-focused with the excitation. In principle, STED microscopy has the advantage of achieving better resolution and utilizing the whole luminescence power due to excitation. In our method, in order to achieve SR only minute fractions of the luminescence power are prevalent in high harmonics (see Supplement 1.1), thus limiting the practical improvement in SR to a factor of 2-3. However, STEND microscopy carries some practical advantages over STED microscopy.

A. It requires only low STED beam intensity (~0.4 I_0 in STEND vs. ~10 I_0 in STED). Whenever bleaching by the STED beam is a problem, our approach is appealing.
B. Out of focus contributions, anti-Stokes emission background typical to STED [36,37], are not modulated and do not interfere with the image.
C. In turbid samples, the purity of the vortex STED beam deteriorates fast with the depth of the interrogation, unlike our Bessel STED beam. This allows in principle SR at larger sample penetration depths than the classical STED microscopy [25].
D. The lack of dedicated wave-plates enables an easy and inexpensive adaptation of the method to any scanning confocal microscope, and provides a very flexible choice of wavelength for excitation and depletion.

Since the contribution to STEND signal comes only from locations in which the excitation and STED beams overlap, super-oscillation beams [38] can be used for the STED beam in order to further enhance resolution. We wish to highlight the fact that we are recording several channels simultaneously, this allows us to obtain the same image in high resolution (but low SNR) along with images of lower resolution but with better SNR. Finally, we wish to emphasize that while STEND is a general SR method, its realization on FNDs testifies for its usefulness for biological and industrial applications in which FNDs are used as markers [39,40].

Funding.

Acknowledgement.

We acknowledge Aviv Swartz for preparing the laser marked ITO coated substrates.

Disclosures. The authors declare no conflicts of interest.

See supplementary materials section 1 for supporting content.

References

1. G. Jacquemet, A. F. Carisey, H. Hamidi, R. Henriques, and C. Leterrier, "The cell biologist's guide to super-resolution microscopy," J. Cell Science **133**, 1-9 (2020).

2. M. Yamanaka, N. I. Smith, and K. Fujita, "Introduction to super-resolution microscopy," Microscopy (Oxf.) **63** (3), 177–192 (2014).

3. E. Abbe, "Beitrage Zur Theorie des Mikroskops Und der Mikroskopischen Wahrnehmung," Arch. Mikrosk. Anat. **9**(1), 413-418 (1873).

4. A. Lewis, H. Taha, A. Strinkovski, A. Manevitch, A. Khatchatouriants, R. Dekhter, and E. Ammann, "Near-field optics: From subwavelength illumination to nanometric shadowing," Nat. Biotechnology **21**(11), 1377–1386 (2003); R. J. Hermann, M. J. Gordon, "Nanoscale Optical Microscopy and Spectroscopy Using Near-Field Probes," Annu. Rev. Chem. Biomol. Eng. **9**(1), 365-387 (2018).

5. T. A. Klar, S. Jakobs, M. Dyba, A. Egner, and S. W. Hell, "Fluorescence microscopy with diffraction resolution barrier broken by stimulated emission," Proc. Natl. Acad. Sci. U.S.A. **97**(15), 8206–8210 (2000).

6. T. A. Klar, E. Engel, and S. Hell, "Breaking Abbe's diffraction resolution limit in fluorescence microscopy with stimulated emission depletion beams of various shapes," Phys. Rev. E **64**, 066613 (2001).

7. R. Henriques, C. Griffiths, E. Hesper Rego, and M. M. Mhlanga, "PALM and STORM: unlocking live-cell super-resolution," Biopolymers **95**(5), 322–331 (2011).

8. M. J. Rust, M. Bates, and X. Zhuang, "Sub-diffraction-limit imaging by stochastic optical reconstruction microscopy (STORM)," Nat. Methods **3**(10), 793–796 (2006).

9. K. Fujita, M. Kobayashi, S. Kawano, M. Yamanaka, and S. Kawata, "High-resolution confocal microscopy by saturated excitation of fluorescence," Phys. Rev. Lett. **99**(22), 228105 (2007).

10. M.G.L. Gustaffson, "Surpassing the lateral resolution limit by a factor of two using structured illumination microscopy," J. Microscopy **198**, 82-87 (2000).

11. T. Dertinger, R. Colyer, G. Iyer, S. Weiss, and J. Enderlein, "Fast, background-free, 3D super-resolution optical fluctuation imaging (SOFI)," Proc. Natl. Acad. Sci. U.S.A. **106**(52), 22287–22292 (2009).

12. O. Schwartz, J. M. Levitt, R. Tenne, S. Itzhakov, Z. Deutsch, and D. Oron, "Superresolution microscopy with quantum emitters," Nano Lett. **13**(12), 5832–5836 (2013).

13. W. Richardson, "Bayesian-based iterative method of image restoration," J. Opt. Soc. of Am. **62**(1), 55–59 (1972).

14. M. G. L. Gustafsson, "Nonlinear structured-illumination microscopy: wide-field fluorescence imaging with theoretically unlimited resolution," Proc. Natl. Acad. Sci. U.S.A. **102**(37), 13081–13086 (2005).

15. Y. Nawa, Y. Yonemaru, A. Kasai, R. Oketani, H. Hashimoto, N. I. Smith, and K. Fujita, "Saturated excitation microscopy using differential excitation for efficient detection of nonlinear fluorescence signals" APL Photonics **3**, 080805(2018).

16. F. Dake, and Y. Taki, "Time-domain fluorescence lifetime imaging by nonlinear fluorescence microscopy constructed of a pump-probe setup with two-wavelength laser pulses," Appl. Opt. **57**(4), 757-762 (2018).

17. F. Dake, N. Fukutake, S. Hayashi, and Y. Taki, “Super-resolving nonlinear fluorescence microscopy with pump–probe setup using repetitive stimulated transition,” Appl. Phys. Express **11**, 012401 (2018).

18 **Fumihiro Dake and Seri Hayashi, "High-resolution nonlinear fluorescence microscopy using repetitive stimulated transition based on the saturation of stimulated emission implemented with two-color continuous-wave lasers," Opt. Lett. 44, 3402-3405 (2019)**

19. S. W. Chu, T. Y. Su, R. Oketani, Y. T. Huang, H. Y. Wu, Y. Yonemaru, M. Yamanaka, H. Lee, G. Y. Zhuo, M. Y. Lee, S. Kawata, and K. Fujita, “Measurement of a Saturated Emission of Optical Radiation from Gold Nanoparticles: Application to an Ultrahigh Resolution Microscope,” Phys. Rev. Lett. **112**(1), 017402 (2014).

20. O. Tzang, A. Pevzner, R. E. Marvel, R. F. Haglund, and O. Cheshnovsky, “Super-resolution in label-free photomodulated reflectivity,” Nano Lett. **15**(2), 1362–1367 (2015).

21. O. Tzang and O. Cheshnovsky, “New modes in label-free super resolution based on photo-modulated reflectivity,” Opt. Express **23**(16), 20926–20932 (2015).

22. E. Ronzitti, B. Harke, and A. Diaspro, “Frequency dependent detection in a STED microscope using modulated excitation light,” Opt. Express **21**(1), 210–219 (2013).

23. M. Castello, G. Tortarolo, I. Coto Hernández, T. Deguchi, A. Diaspro, and G. Vicidomini, “Removal of anti-Stokes emission background in STED microscopy by FPGA-based synchronous detection,” Rev. Sci. Instrum. **88**, 053701 (2017).

24. L. Lanzanò, I. Coto Hernández, M. Castello, E. Gratton, A. Diaspro, and G. Vicidomini, “Encoding and decoding spatio-temporal information for super-resolution microscopy,” Nat. Commun. **6**(1), 6701 (2015).

25. B. R. Patton, D. Burke, D. Owald, T. J. Gould, J. Bewersdorf, and M. J. Booth, “Three-dimensional STED microscopy of aberrating tissue using dual adaptive optics,” Opt. Express **24**(8), 8862–8876 (2016).

26. M. Berthel, O. Mollet, G. Dantelle, T. Gacoin, S. Huant, and A. Drezet, “Photophysics of single nitrogen-vacancy centers in diamond nanocrystals,” Phys. Rev. B **91**, 035308 (2015).

27. K. Y. Han, K. I. Willig, E. Rittweger, F. Jelezko, C. Eggeling, and S. W. Hell, “Three-dimensional stimulated emission depletion microscopy of nitrogen-vacancy centers in diamond using continuous-wave light,” Nano Lett. **9**(9), 3323–3329 (2009).

28. S. Arroyo-Camejo, M.-P. Adam, M. Besbes, J.-P. Hugonin, V. Jacques, J.-J. Greffet, J.-F. Roch, S. W. Hell, and F. Treussart, “Stimulated emission depletion microscopy resolves individual nitrogen vacancy centers in diamond nanocrystals,” ACS Nano **7**(12), 10912–10919 (2013).

29. K. I. Willig, B. Harke, R. Medda, and S. W. Hell, “STED microscopy with continuous wave beams,” Nat. Methods **4**(11), 915–918 (2007).

30. R. Ulbricht and Z. H. Loh, "Excited-state lifetime of the NV− infrared transition in diamond," Phys. Rev. B. **98**, 094309 (2018).

31. O. Tzang, D. Hershkovitz and O. Cheshnovsky, "Pure sinusoidal photo-modulation using an acousto-optic modulator" Rev. Sci. Inst. **89**, 123102 (2018).

32. C. B. Müller and J. Enderlein, "Image scanning microscopy," Phys. Rev. Lett. **104**(19), 198101 (2010).

33. G. P. J. Laporte, N. Stasio, C. J. R. Sheppard, and D. Psaltis, "Resolution enhancement in nonlinear scanning microscopy through post-detection digital computation," Optica **1**(6), 455–460 (2014).

34. I. Gregor, M. Spiecker, R. Petrovsky, J. Großhans, R. Ros, and J. Enderlein, "Rapid nonlinear image scanning microscopy," Nat. Methods **14**(11), 1087-1089 (2017).

35. R. Tenne, U. Rossman, B. Rephael, Y. Israel, A. Krupinski-Ptaszek, R. Lapkiewicz, Y. Silberberg, and D. Oron, "Super-resolution enhancement by quantum image scanning microscopy," Nat. Photonics **13**(2), 116–122 (2019).

36. I. Coto Hernàndez, C. Peres, F. Cella Zanacchi, M. d'Amora, S. Christodoulou, P. Bianchini, A. Diaspro, and G. Vicidomini, "A new filtering technique for removing anti-Stokes emission background in gated CW-STED microscopy," J. Biophotonics **7**(6), 376–380 (2014).

37. J. C. Lee, Y. Ma, K. Y. Han, and T. Ha, "Accurate background subtraction in STED nanoscopy by polarization Switching," ACS Photonics, **6**(7), 1789–1797 (2019).

38 Optical super-oscillations: sub-wavelength light focusing and super-resolution imagingEdward T F Rogers and Nikolay I Zheludev 2013 J. Opt. 15 094008

39. S. Chauhan, N. Jain and U. Nagaich, "Nanodiamonds with powerful ability for drug delivery and biomedical applications: Recent updates on in vivo study and patents," J. Pharm. Anal. **10**(1), 1-12 (2020).

40. M. H. Alkahtani, F. Alghannam, L. Jiang, A. Almethen, A. A. Rampersaud, R. Brick, C. L. Gomes, M. O. Scully, and P. R. Hemmer, "Fluorescent nanodiamonds: past, present, and future," Nanophotonics **7**(8), 1423–1453 (2018).